J. Fluid Mech. (2010), *vol.* 656, *pp.* 530–539.
doi:10.1017/S0022112010002442

On unified boundary conditions for improved predictions of near-wall turbulence

S. JAKIRLIĆ[1,3]† AND J. JOVANOVIĆ[2,3]

[1]Institute of Fluid Mechanics and Aerodynamics, Technische Universität Darmstadt, Petersenstrasse 30, D-64287 Darmstadt, Germany

[2]Institute of Fluid Mechanics, Friedrich-Alexander University of Erlangen-Nuremberg, Cauerstrasse 4, D-91058 Erlangen, Germany

[3]Center of Smart Interfaces, Technische Universität Darmstadt, Petersenstrasse 32, D-64287 Darmstadt, Germany

(Received 9 December 2009; revised 9 April 2010; accepted 21 April 2010; first published online 1 July 2010)

A novel formulation of the wall boundary conditions relying on the asymptotic behaviour of the Taylor microscale λ and its relationship to the homogeneous part of the viscous dissipation rate of the kinetic energy of turbulence $\epsilon_h = 5\nu q^2/\lambda^2$, applicable to near-wall turbulence, is examined. The linear dependence of λ on the wall distance in close proximity to the solid surface enables the wall-closest grid node to be positioned immediately below the edge of the viscous sublayer, leading to a substantial coarsening of the grid resolution. This approach provides bridging of a major portion of the viscous sublayer, higher grid flexibility and weaker sensitivity against the grid non-uniformities in the near-wall region. The performance of the proposed formulation was checked against available direct numerical simulation databases of complex wall-bounded flows featured by swirl and separation.

Key words: turbulence modelling, wall-bounded flows

1. Introduction

One of the most important achievements in turbulence research is certainly the 'law of the wall', implying that the wall-parallel mean velocity field follows a simple logarithmic distribution: $U^+ = \ln(Ey^+)/\kappa$ (with $U^+ = U/U_\tau$, $y^+ = U_\tau y/\nu$), where $U_\tau = \sqrt{\tau_w/\rho}$ and $\tau_w = \mu(\partial U/\partial y)_{y=0}$ are the friction velocity and the wall shear stress, respectively. For fully developed zero-pressure-gradient boundary-layer flows, the most widely used values for the coefficients are $\kappa \approx 0.41$ and $E \approx 7.768$–8.432 (Bradshaw 1978).

The law of the wall and two associated features, equality of the production rate of the kinetic energy of turbulence and its dissipation rate (known as 'local equilibrium') $P_k \simeq \epsilon$, and the uniformity of the turbulent shear stress, $\rho\overline{uv}$, which is nearly equal to the wall shear stress τ_w (across 'constant stress layer' $\overline{uv}/U_\tau^2 \simeq 1$), constitute the rationale of the widely used 'high-Reynolds-number wall functions', which were originally proposed by Launder & Spalding (1974). The wall functions, used in conjunction with turbulence models at high Reynolds numbers, can be applied provided that the wall-closest computational node is situated in the equilibrium region (say $y^+ \geqslant 30$). In such a way, the viscosity-affected immediate wall vicinity is entirely

† Email address for correspondence: s.jakirlic@sla.tu-darmstadt.de

bridged and therefore the details of the mean flow and turbulence fields in the wall-adjacent flow region are completely missed. The use of the wall function concept is justified only in equilibrium flows whose features comply with the assumptions mentioned above. The validity of this concept in non-equilibrium flows is therefore considered to be inappropriate, particularly in separating flows, around reattachment, in the presence of strong pressure gradients or rotation. Correct capture of these phenomena can be achieved only by integration of the modelled equations up to the wall using the exact boundary conditions. However, this approach requires very fine near-wall resolution of the order of $y^+ \leqslant 0.5$–1.0, which is very demanding to fulfil in the entire flow domain of complex three-dimensional flows at higher Reynolds numbers, as e.g. in car or aircraft configurations. For the computations of such flows, this means in practice an increase in grid resolution by at least a factor of 2 or even more compared with corresponding calculations based on the application of wall functions. The necessity for a fine grid in the immediate wall vicinity arises from the fact that the structure of the turbulent transport equations is extremely complex in the viscous sublayer region where the turbulence quantities exhibit steeper gradients which must be appropriately resolved by the numerical grid. The grid refinement in the normal-to-wall direction causes extremely elongated near-wall grid cells with higher aspect ratio leading to slower convergence of numerical procedures.

Apart from the demanding requirement for high grid resolution, an even more complicated situation is related to coupling between the transport equations for the turbulent dissipation rate and the turbulent stresses when turbulence approaches the two-component state near the wall, $\epsilon_{ij} \rightarrow \nu \partial^2 \overline{u_i u_j}/\partial x_k \partial x_k$ as $y \rightarrow 0$. This coupling, which cannot be avoided by any simple (and naive) transformation, as a rule causes numerical instabilities or very poor convergence in computations of flows involving complex geometries. In addition to this difficulty, which prevents the formulation of numerically robust boundary conditions at the wall, the extreme sensitivity of the decay term $-\psi\, k^2/\epsilon$ of the model equation for the turbulent dissipation rate to huge variations in anisotropy in the viscous sublayer, where turbulence can sweep between the two-component isotropic state to the one-component state, prevents reliable predictions of the dissipation rate at the wall where it reaches the maximum value from its own transport equation (Jovanović 2004).

The activity on development of the more universal wall boundary conditions, blending between the integration up to the wall and high-Reynolds-number wall function approach, has recently experienced substantial intensification (see Esch & Menter 2003; Popovac & Hanjalic 2007). The latter authors proposed the generalized wall functions that include non-equilibrium effects as the upper bound. In connection with this issue, it is worth mentioning the work of Craft *et al.* (2004) on the development of the more sophisticated wall functions relying on the integration of the parabolized form of the governing equations across the locally refined wall-adjacent grid cell.

In the present work, we propose a solution for both the physical modelling and numerical implementation of the wall-boundary conditions, which should permit the advantageous use of the second-moment and related turbulence closures for prediction of flows near solid boundaries for complex and technically relevant applications. The wall-closest grid node is positioned close to the edge of the viscous sublayer, which allows higher grid flexibility and weaker sensitivity against the grid non-uniformities in the near-wall regions. The basis of the present procedure is the asymptotic behaviour of the Taylor microscale λ in the limit when $y \rightarrow 0$ resulting in the linear dependence of λ on the wall distance y.

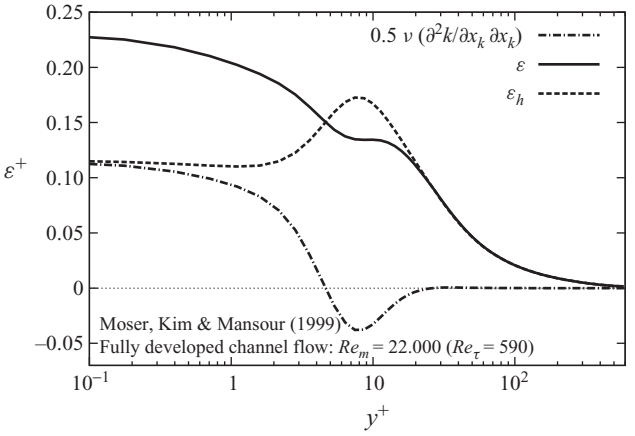

FIGURE 1. Total viscous dissipation rate ϵ split into the homogeneous part ϵ_h and the inhomogeneous part $0.5\nu(\partial^2 k/\partial x_k\,\partial x_k)$.

2. The asymptotic behaviour of the Taylor microscale near the wall

The detailed theoretical foundation of the Taylor microscale, λ, can be found in classical papers by Taylor (1935) and Chou (1945) (see Jovanović 2004). The starting point of the present analysis is the relationship between the turbulent dissipation rate ϵ, kinetic energy of turbulence k ($2k = \overline{u_i u_i} = q^2$) and the Taylor microscale, which reads as follows:

$$\epsilon_h = 5\nu \frac{q^2}{\lambda^2}, \tag{2.1}$$

for the case of homogeneous turbulence (see figure 1 and corresponding discussion). The Taylor microscale λ represents an intermediate length scale related to the overlapping region between the energy-containing part of the turbulence spectrum and its dissipative complement. The asymptotic behaviour of λ near solid boundaries follows from the series expansion of the instantaneous velocity fluctuations around the wall $u_i = a_i + b_i y + c_i y^2 + \cdots$, where coefficients a_i, b_i and c_i represent functions of x, z and time t. By accounting for the non-slip boundary condition at the wall, $(u)_{y=0} = (v)_{y=0} = (w)_{y=0} = 0 \Rightarrow a_i = 0$, and for the continuity equation, $\partial u/\partial x + \partial v/\partial y + \partial w/\partial z = 0 \Rightarrow b_2 = 0$, the following expressions for the Reynolds stress components, kinetic energy of turbulence and the turbulent dissipation rate are obtained:

$$\left.\begin{aligned}
\overline{u^2} &= \overline{u_1 u_1} = \overline{b_1 b_1} y^2 + 2\overline{b_1 c_1} y^3 + \cdots, \\
\overline{v^2} &= \overline{u_2 u_2} = \overline{c_2 c_2} y^4 + \cdots, \\
\overline{w^2} &= \overline{u_3 u_3} = \overline{b_3 b_3} y^2 + 2\overline{b_3 c_3} y^3 + \cdots, \\
\overline{uv} &= \overline{u_1 u_2} = \overline{b_1 c_2} y^3 + \cdots, \\
k &= \tfrac{1}{2}\overline{u_i u_i} = \tfrac{1}{2}\left(\overline{u^2} + \overline{v^2} + \overline{w^2}\right) \\
&= \tfrac{1}{2}\left(\overline{b_1 b_1} + \overline{b_3 b_3}\right) y^2 + \left(\overline{b_1 c_1} + \overline{b_3 c_3}\right) y^3 + \cdots, \\
\epsilon &= \nu \overline{\frac{\partial u_i}{\partial x_k}\frac{\partial u_i}{\partial x_k}} = \nu\left(\overline{b_1 b_1} + \overline{b_3 b_3}\right) + 4\nu\left(\overline{b_1 c_1} + \overline{b_3 c_3}\right) y + \cdots.
\end{aligned}\right\} \tag{2.2}$$

Using the two-point correlation technique, the turbulent dissipation rate, ϵ, can be split into the homogeneous part, ϵ_h, and the inhomogeneous part as follows (Jovanovic, Ye & Durst 1995):

$$\epsilon = \epsilon_h + \frac{1}{2}\nu\frac{\partial^2 k}{\partial x_k \partial x_k}. \tag{2.3}$$

The graphical representation of this expression is given in figure 1, which clearly illustrates the difference between ϵ and ϵ_h. The inhomogeneous part of ϵ is pertinent only to the immediate wall vicinity up to $y^+ \approx 20$–30. Utilizing the homogeneous dissipation rate as a scale-determining variable has a number of important advantages compared with the total dissipation rate, which has being commonly used in most existing turbulence models. The modelled form of the transport equation for the homogeneous part of the dissipation rate provides a proper near-wall shape of the dissipation rate profile without introducing any additional term and the correct asymptotic behaviour of the stress dissipation components ϵ_{ij} by approaching the solid wall without the necessity for any wall geometry-related parameter (Jakirlic & Hanjalic 2002). The asymptotic behaviour of the Taylor microscale near the wall is closely connected to the near-wall behaviour of the homogeneous part of the dissipation rate and is obtained from (2.3) using the series expansions (2.2) for ϵ and k:

$$\epsilon_h = \tfrac{1}{2}\nu\left(\overline{b_1 b_1} + \overline{b_3 b_3}\right) + \nu\left(\overline{b_1 c_1} + \overline{b_3 c_3}\right) y + \cdots \tag{2.4}$$

resulting, from application of (2.1), in a linear dependence on the wall distance:

$$\lambda = \sqrt{10}y + \cdots, \quad y \to 0. \tag{2.5}$$

3. Validation using numerical databases

The linear variation of the Taylor microscale in terms of wall distance in the near-wall region and associated behaviour of the viscous dissipation of the kinetic energy of turbulence is illustrated graphically in figures 2 and 3, displaying the relationship between λ, k and ϵ_h obtained from (2.1), (2.3) and (2.5) in different wall-bounded flows for which a detailed database is available from direct numerical simulations (DNS) of fully developed channel flow (Moser, Kim & Mansour 1999; Tanahashi *et al.* 2004; Hoyas & Jimenez 2006), flow in an axially rotating pipe (Orlandi & Ebstein 2000 as representative of the swirling flows with underlying transverse streamline curvature effects) and flow over a backward-facing step (Le, Moin & Kim 1997 as representative of a complex flow configuration being characterized by differently structured flow regions affected globally by an adverse pressure gradient due to cross-section expansion: boundary-layer separation, separated shear layer impingement on the step wall at the reattachment region followed by flow bifurcation, recirculation zone, post-reattachment recovery region and the newly developing boundary layer). These numerical results correspond to a wide range of Reynolds numbers Re_m (based on the bulk velocity and the full channel height $Re_m = U_m 2h/\nu$) and different rotational intensities N (where N represents the ratio between the circumferential wall velocity and the bulk velocity, $N = W_{wall}/U_m$).

The λ profiles, obtained from (2.1) and (2.3) by utilizing the numerical data for ϵ and q^2, exhibit linear behaviour across the entire viscous sublayer and match perfectly among each other independently of the Reynolds number, rotational intensity and

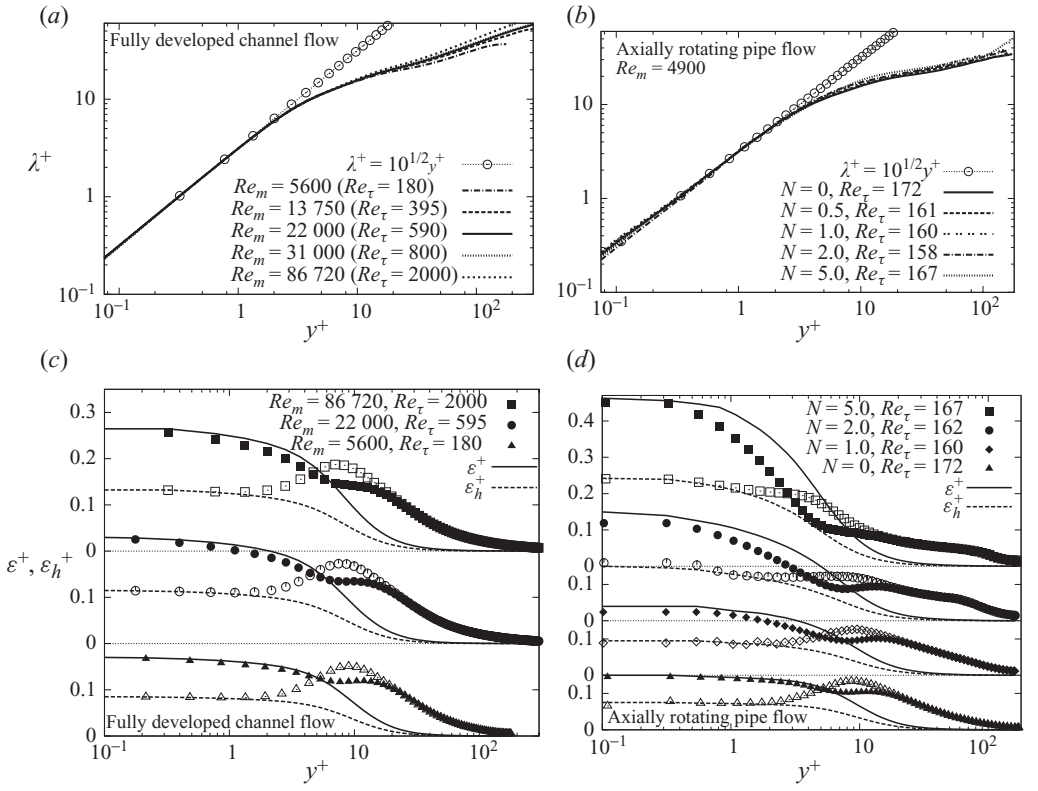

FIGURE 2. Near-wall behaviour of Taylor microscale λ^+ (a, b) and the dissipation rate profiles ϵ^+ and ϵ_h^+ (c, d) in a fully developed plane channel flow in a range of Reynolds numbers (a, c) and in an axially rotating pipe flow for different rotational intensities N (b, d). Symbols represent DNS results of the channel flow from Moser, Kim & Mansour (1999) ($Re_\tau = 180$, 395 and 590), Tanahashi *et al.* (2004) ($Re_\tau = 800$) and Hoyas & Jimenez (2006) ($Re_\tau = 2000$) and of the rotating pipe flow from Orlandi & Ebstein (2000). Here ϵ^+ is plotted with filled symbols and ϵ_h^+ with empty symbols. The data are normalized with the inner variables as $\lambda^+ = U_\tau \lambda/\nu$ and $\epsilon^+ = \epsilon\nu/U_\tau^4$.

the flow region in the backward-facing step flow. There is a high level of agreement to a wall distance in the range $y^+ \approx 3$ for the channel flow in the entire investigated Reynolds number range. A similar situation is observed in an axially rotating pipe flow if the rotational intensity range corresponds to $N \leqslant 1.0$. A certain deviation with increasing rotation ($N \geqslant 2.0$) is obvious, but it is not of decisive importance with respect to practical usage of λ. Very good agreement in the near-wall layer pertinent to all characteristic regions of a separated flow, including the recirculation zone, reattachment and recovery regions, is obtained in the flow over a backward-facing step, as can be concluded from figure 3(a). We may also add in passing that the range of validity of the wall boundary conditions arising from this analysis can be somewhat expanded from the point of view of their practical application, as can be seen in the computations using the complete turbulence model, shown in figures 6 and 7. Figure 2(c, d) and figure 3(b) emphasize the difference between ϵ and ϵ_h, which is noticeable only in the near-wall region. The ϵ_h profiles are obtained from (2.1), with λ following from expression (2.5), and ϵ profiles from (2.3) using the results for k from numerical databases as input variable. The dissipation profiles obtained in

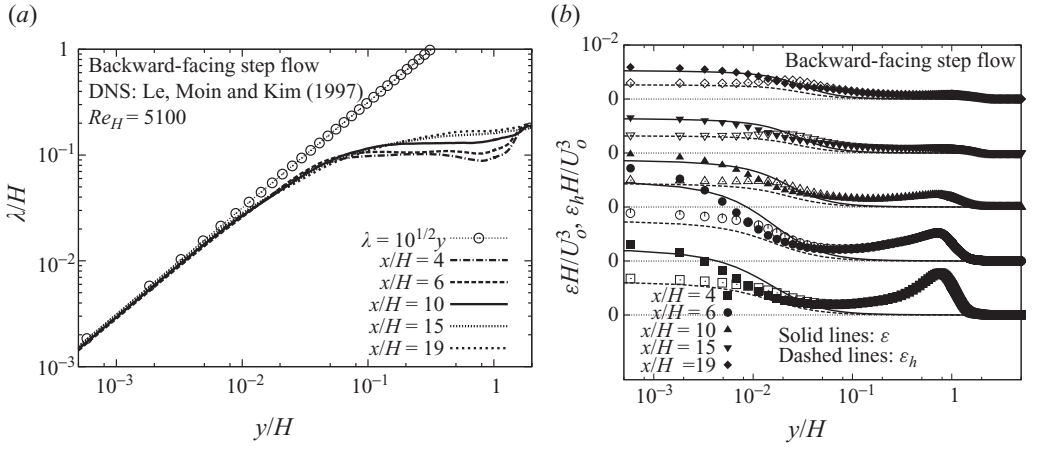

FIGURE 3. The near-wall behaviour of Taylor microscale λ (a) and dissipation rate profiles ϵ and ϵ_h (b) in the backward-facing step flow. Here H is the step height and $x/H = 4$ corresponds to the recirculation region, $x/H = 6$ to the reattachment region and $x/H = 10$, 15 and 19 to the recovery region. Symbols represent numerical results from Le, Moin & Kim (1997).

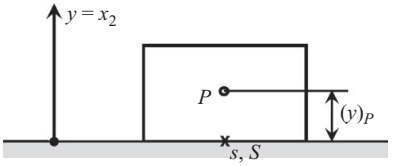

FIGURE 4. The wall-adjacent grid cell.

such a way match correctly their DNS wall values. Moreover, very good agreement is noticeable up to the wall distance being in the range $y^+ \approx 3$–5.

The above discussion suggests that wall boundary conditions to be used in the framework of near-wall turbulence models can be conveniently realized with the following procedure:

(a) The wall-closest numerical node has to be situated in the viscous sublayer where the linear velocity law $U^+ = y^+$ holds. It is important to note that in equilibrium flows the edge of the viscous sublayer is located at $y^+ \approx 5$ but it deviates from this value in non-equilibrium flows.

(b) The Taylor microscale λ is evaluated at the wall-adjacent node $\boldsymbol{P}$ (as shown in figure 4) from

$$\lambda_P = \sqrt{10}(y)_P. \tag{3.1}$$

(c) The homogeneous part of the turbulent dissipation rate is computed as follows:

$$(\epsilon_h)_P = 10\nu k_P/\lambda_P^2. \tag{3.2}$$

(d) The boundary conditions at the wall for the kinetic energy of turbulence k and individual stress components $\overline{u_i u_j}$ follow from zero values of their gradients at $y = 0$, which can be concluded from (2.2):

$$\frac{\partial k}{\partial y}, \frac{\partial \overline{u^2}}{\partial y}, \frac{\partial \overline{v^2}}{\partial y}, \frac{\partial \overline{w^2}}{\partial y}, \frac{\partial \overline{uv}}{\partial y} \quad \text{and also} \quad \frac{\partial \overline{uw}}{\partial y}, \frac{\partial \overline{vw}}{\partial y}. \tag{3.3}$$

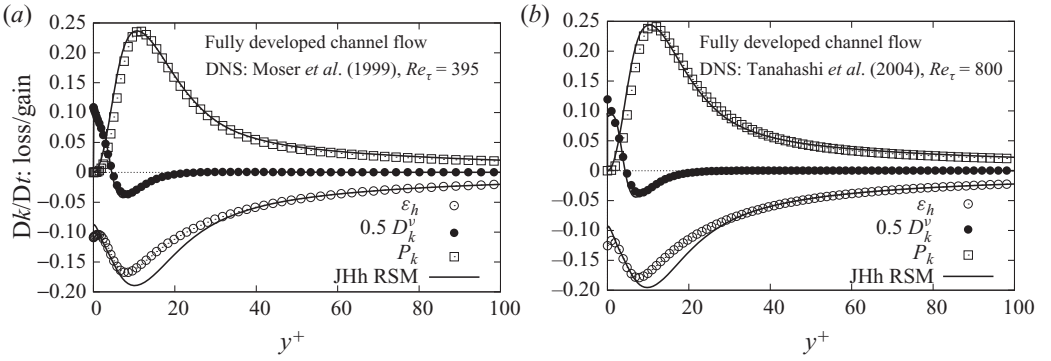

FIGURE 5. Production rate ($P_k = -\overline{u_i u_j}\partial U_i/\partial x_j$) and homogeneous ($\epsilon_h$) and inhomogeneous ($0.5D_k^v$) dissipation rates in the budget of the transport equation of kinetic energy of turbulence k in the fully developed channel flow at $Re_\tau = 395$ and $Re_\tau = 800$. 'JHh RSM' denotes the Reynolds stress model based on the homogeneous dissipation concept by Jakirlic & Hanjalic (2002).

As the node $\boldsymbol{P}$ is still fairly close to the wall, where the series expansions (2.2) hold, integration of the equations governing the Reynolds stress components using (3.3) is equivalent to Dirichlet boundary conditions by setting zero wall values for the stresses at the node $\boldsymbol{s}$ (as shown in figure 4).

Similarly to the 'high-Reynolds-number wall functions' comprising of a set of constraints for the turbulence quantities at the beginning of the equilibrium region, the above formulations can therefore be termed the 'low-Reynolds-number wall functions'.

4. Numerical predictions of simple and complex wall-bounded flows

The feasibility of the proposed wall boundary conditions (3.1), (3.2) and (3.3) is demonstrated by computing fully developed channel flow at the bulk Reynolds numbers $Re_m = 13\,750$ and $Re_m = 31\,000$ (corresponding to $Re_\tau = 395$ and $Re_\tau = 800$, studied numerically by Moser, Kim & Mansour 1999 and Tanahashi *et al.* 2004, respectively) and a backward-facing step flow at the step-height Reynolds number $Re_H = 5100$ (investigated by Jovic & Driver 1995; Le, Moin & Kim 1997) in conjunction with the near-wall second moment closure proposal by Jakirlic & Hanjalic (2002) based on the homogeneous dissipation concept (denoted by JHh in figures 5 and 7). Accordingly, the transport equation for the Reynolds stress tensor is solved in conjunction with the scale-supplying equation governing the homogeneous dissipation rate ϵ_h. As the inhomogeneous part of the total turbulent dissipation rate corresponds exactly to half of the molecular diffusion of the kinetic energy of turbulence, $D_k^v = \nu\partial^2 k/(\partial x_k \partial x_k)$ (see (2.3) and associated discussion), it does not have to be modelled. Hence, the total turbulent dissipation rate does not appear in the final model formulation and should not be considered further. Figure 5 illustrates the comparison of the DNS results and computed terms in the budget of the equation of the kinetic energy of turbulence: production rate P_k and both homogeneous (ϵ_h) and inhomogeneous ($D_k^v/2$) dissipation rates in the plane channel flow at two above-mentioned Reynolds numbers. Interested readers are referred to the work of Jakirlic and Hanjalic (2002) for the complete specification of the differential Reynolds stress model employed. It should be pointed out that this model was selected just in order to illustrate the performances of the presently formulated wall boundary conditions in the framework of the computations using the complete set of equations for all stress

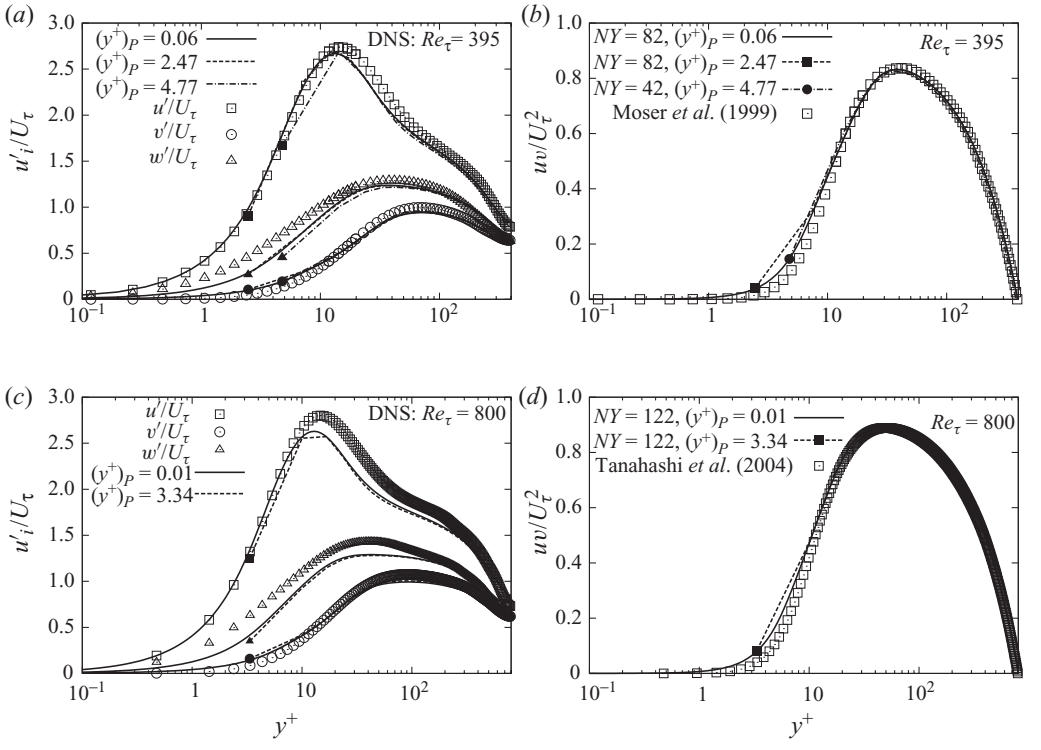

FIGURE 6. Numerical predictions resulting from application of wall boundary conditions (3.1), (3.2) and (3.3) to a fully developed channel flow: normal stress components (*a*, *c*) and shear stress (*b*, *d*). DNS results are from Moser, Kim & Mansour (1999) ($Re_\tau = 395$, $Re_m = 13\,750$) and Tanahashi *et al.* (2004) ($Re_\tau = 800$, $Re_m = 31\,000$). Here the $(y^+)_P$ values correspond to the wall-adjacent node and NY denotes the number of grid points in the y direction over the channel half-width h.

components. The main objective is to show that the predicted results away from the viscous sublayer, independently of the position of the wall-adjacent computational node, coincide with those obtained by setting $y_P^+ < 1$. It should furthermore be emphasized that the present wall boundary conditions can be used in conjunction with any scale-supplying variable, i.e. scale-supplying equation – governing either the total turbulent dissipation rate or its homogeneous part; it could also be extended to any quantity of the general form $\epsilon^m k^n$ (e.g. $m = 1$, $n = -1 \Rightarrow \epsilon/k = \omega$ – inverse time scale). Accordingly, they are independent of the turbulence model applied. Both the eddy-viscosity model group and Reynolds stress models can be considered.

Selected results shown in figures 6 and 7 depict the behaviour of all important quantities representing typically the results of flow predictions: mean velocities, all four turbulent stress components and the skin-friction coefficient C_f, representing the integral flow characteristic of great practical importance, under the conditions of grid coarsening with respect to the wall-closest grid node. Their behaviour is analogous in other wall-bounded flow configurations. The solid lines represent the results obtained by applying the conventional near-wall boundary conditions, which requires very small values for $(y^+)_P$ for the wall-adjacent grid node. The results obtained on coarser grids for which the proposed wall boundary conditions were applied follow closely the results obtained on the finest grid in the remaining part

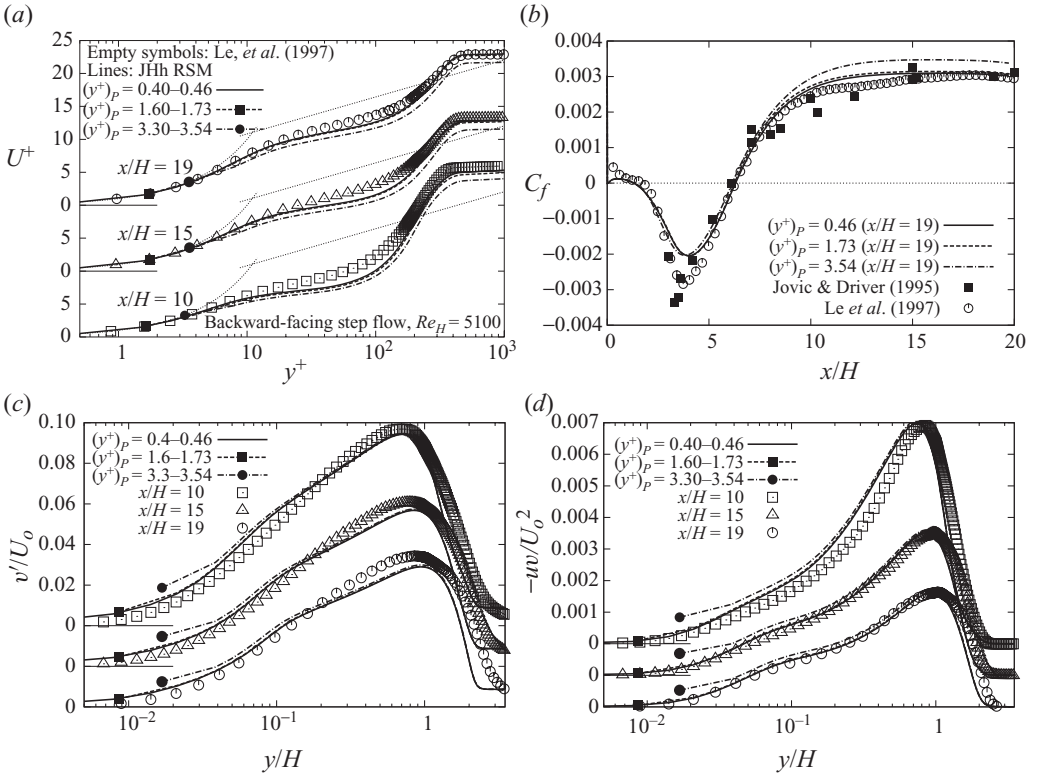

FIGURE 7. Numerical predictions of a backward-facing step flow obtained by application of proposed wall boundary conditions: mean velocity and Reynolds stress component ($v' = \sqrt{\overline{v^2}}$ and $\overline{uv}$) profiles in the recovery region and skin friction coefficient. Symbols correspond to the DNS results of Le *et al.* (1997). JHh RSM denotes the Reynolds stress model based on the homogeneous dissipation concept by Jakirlic & Hanjalic (2002).

of the cross-section. The $(y^+)_P = 4.77$ value of the wall-closest grid point implies the application of these boundary conditions at the viscous sublayer edge in the plane channel flow. A similar degree of agreement is obtained by applying the proposed wall boundary conditions in the flow over a backward-facing step shown in figure 7. The coarsest grid used corresponds to $(y^+)_P = 3.30$–3.54 at the streamwise locations $x/H = 10$, 15 and 19 in the post-reattachment region. The predicted results exhibit a certain departure from those obtained on finer grids, this being especially visible when analyzing the friction factor development. However, this deviation is caused solely by the wall-closest grid point lying outside the $U^+ = y^+$ validity range, whose upper bound corresponds to $y^+ \approx 2.5$ for the streamwise locations considered in the recovery region.

5. Conclusion

The exact linear behaviour of the Taylor microscale in the immediate wall vicinity, corresponding to $\lambda = \sqrt{10}y + \cdots$, representing a unique property of differently featured wall-bounded flow configurations, and the related exact relationship to the homogeneous part of the turbulent dissipation rate $\epsilon_h = 10\nu k/\lambda^2$ represent the basis for formulation of the unified wall boundary conditions pertinent to the low-Reynolds-number

turbulence models. Their application permits significant coarsening of the near-wall grid resolution (leading also to a more convenient cell aspect ratio), enabling the wall-adjacent computational node to be located at the edge of the viscous sublayer. The most important benefit of their use is a weaker grid sensitivity to the grid size in complex wall-bounded configurations with flow passing differently characterized regions, e.g. transition from attached to separated flow regions or the opposite.

This work was sponsored in part by the Center of Smart Interfaces at Technische Universität Darmstadt and in part by the grants Jo 240/5-3 and SFB 568 (TPC3) from the Deutsche Forschungsgemeinschaft. The authors gratefully acknowledge the above-mentioned sponsorships.

REFERENCES

Bradshaw, P. 1978 Turbulence – Introduction. In *Topics in Applied Physics: Turbulence* (ed. P. Bradshaw), vol. 12, pp. 1–44. Springer.

Chou, P. Y. 1945 On the velocity correlation and the solution of the equation of turbulent fluctuations. *Q. Appl. Math.* **3**, 38–54.

Craft, T. J., Gant, S. E., Iacovides, H. & Launder, B. E. 2004 A new wall function strategy for complex turbulent flows. *Numer. Heat Transfer, Part* B*: Fundam.* **45** (4), 301–318.

Esch, T. & Menter, R. F. 2003 Heat transfer predictions based on two-equation turbulence models with advanced wall treatment. In *Turbulence, Heat and Mass Transfer* (ed. K. Hanjalic, Y. Nagano & M. Tummers), vol. 4, pp. 633–640. Begell House Inc.

Hoyas, S. & Jimenez, J. 2006 Scaling of the velocity fluctuations in turbulent channels up to $Re_\tau = 2003$. *Phys. Fluids* **18**, 011702.

Jakirlić, S. & Hanjalić, K. 2002 A new approach to modeling near-wall turbulence energy and stress dissipation. *J. Fluid Mech.* **539**, 139–166.

Jovanović, J. 2004 *The Statistical Dynamics of Turbulence*. Springer.

Jovanović, J., Ye, Q.-Y. & Durst, F. 1995 Statistical interpretation of the turbulent dissipation rate in wall-bounded flows. *J. Fluid Mech.* **293**, 321–347.

Jović, S. & Driver, D. 1995 Reynolds number effect on the skin friction in separated flows behind a backward-facing step. *Exp. Fluids* **18**, 464–467.

Launder, B. E. & Spalding, D. B. 1974 The numerical computation of turbulent flows. *Comput. Methods Appl. Mech. Engng* **3**, 269–289.

Le, H., Moin, P. & Kim, J. 1997 Direct numerical simulation of turbulent flow over a backward-facing step. *J. Fluid Mech.* **330**, 349–374.

Moser, R. D., Kim., J. & Mansour, N. N. 1999 Direct numerical simulation of turbulent channel flow up to $Re_\tau = 590$. *Phys. Fluids* **11**, 943–945.

Orlandi, P. & Ebstein, D. 2000 Turbulent budgets in rotating pipe by DNS. *Intl J. Heat Fluid Flow* **21**, 499–505.

Popovac, M. & Hanjalić, K. 2007 Compound wall treatment for RANS computation of complex turbulent flows and heat transfer. *Flow Turbul. Combust.* **78**, 177–202.

Tanahashi, M., Kang, S.-J., Miyamoto, S., Shiokawa, S., & Miyauchi, T. 2004 Scaling law of fine scale eddies in turbulent channel flows up to $Re_\tau = 800$. *Intl J. Heat Fluid Flow* **25**, 331–340.

Taylor, G. I. 1935 Statistical theory of turbulence. *Proc. R. Soc.* A **151**, 421–478.